Published in final edited form as:

Mol Pharmacol. 2008 July ; 74(1): 213–224. doi:10.1124/mol.108.045997.

N-Palmitoyl Glycine, a Novel Endogenous Lipid That Acts As a Modulator of Calcium Influx and Nitric Oxide Production in Sensory Neurons[S]

Neta Rimmerman[#], **Heather B. Bradshaw**[#], **H. Velocity Hughes**, **Jay Shih-Chieh Chen**, **Sherry Shu-Jung Hu**, **Douglas McHugh**, **Eivind Vefring**, **Jan A. Jahnsen**, **Eric L. Thompson**, **Kim Masuda**, **Benjamin F. Cravatt**, **Sumner Burstein**, **Michael R. Vasko**, **Anne L. Prieto**, **David K. O'Dell**, **J. Michael Walker**

Department of Psychological and Brain Sciences (N.R., H.B.B., H.V.H., J.S.-C.C., S.S.-J.H., D.M., E.V., J.A.J., A.L.P., J.M.W.), The Gill Center for Biomolecular Sciences (N.R., H.B.B., H.V.H., J.S.-C.C., S.S.-J.H., D.M., E.V., J.A.J., D.K.O., J.M.W.), and the Kinsey Institute for Research in Sex, Gender and Reproduction (H.B.B.), Indiana University, Bloomington, Indiana; Department of Chemical Physiology, The Scripps Institute, La Jolla, California (K.M., B.F.C.); Department of Pharmacology and Toxicology, Indiana University School of Medicine, Indianapolis, Indiana (E.L.T., M.R.V.); and Department of Biochemistry and Molecular Pharmacology, University of Massachusetts Medical School, Worcester, Massachusetts (S.B.)

[#] These authors contributed equally to this work.

Abstract

N-arachidonoyl glycine is an endogenous arachidonoyl amide that activates the orphan G protein-coupled receptor (GPCR) GPR18 in a pertussis toxin (PTX)-sensitive manner and produces antinociceptive and anti-inflammatory effects. It is produced by direct conjugation of arachidonic acid to glycine and by oxidative metabolism of the endocannabinoid anandamide. Based on the presence of enzymes that conjugate fatty acids with glycine and the high abundance of palmitic acid in the brain, we hypothesized the endogenous formation of the saturated *N*-acyl amide *N*-palmitoyl glycine (PalGly). PalGly was partially purified from rat lipid extracts and identified using nano-high-performance liquid chromatography/hybrid quadrupole time-of-flight mass spectrometry. Here, we show that PalGly is produced after cellular stimulation and that it occurs in high levels in rat skin and spinal cord. PalGly was up-regulated in fatty acid amide hydrolase knockout mice, suggesting a pathway for enzymatic regulation. PalGly potently inhibited heat-evoked firing of nociceptive neurons in rat dorsal horn. In addition, PalGly induced transient calcium influx in native adult dorsal root ganglion (DRG) cells and a DRG-like cell line (F-11). The effect of PalGly on the latter cells was characterized by strict structural requirements, PTX sensitivity, and dependence on the presence of extracellular calcium. PalGly-induced calcium influx was blocked by the nonselective calcium channel blockers ruthenium red, 1-(-[3-(4-methoxyphenyl)propoxy]-4-methoxyphenethyl)-1*H*-imidazole (SK&F96365), and La^{3}. Furthermore, PalGly contributed to the production of NO through calcium-sensitive nitric-oxide

Address correspondence to: Dr. Heather B. Bradshaw, 1101 East 10th St. Bloomington, IN 47405. hbbradsh@indiana.edu.

[S]The online version of this article (available at http://molpharm.aspetjournals.org) contains supplemental material.

synthase enzymes present in F-11 cells and was inhibited by the nitric-oxide synthase inhibitor 7-nitroindazole.

Collectively, the acyl amides constitute a family of ubiquitous endogenous lipids present in varying levels throughout the body (for review, see Di Marzo et al., 2007). These lipids are now recognized as potent modulators of pain and inflammation (Bradshaw and Walker, 2005; Hohmann et al., 2005). The subfamily of arachidonoyl amides is composed of amide-conjugates of ethanolamine, glycine, dopamine, alanine, GABA, serine, and taurine with arachidonic acid (Devane et al., 1992; Huang et al., 2001, 2002; Milman et al., 2006; Saghatelian et al., 2006). The earliest and best characterized among these is *N*-arachidonoyl ethanolamine (AEA; anandamide), an endogenous mammalian homolog to the analgesic phytocannabinoid Δ^9-tetrahydrocannabinol (Devane et al., 1992). AEA activates the G protein-coupled receptors (GPCR) cannabinoid receptor 1 and 2 (CB_1 and CB_2), GPR55, and the transient receptor potential vanilloid (TRPV) type-1 receptor (TRPV1; Devane et al., 1992; Ross, 2003; Ryberg et al., 2007). An oxygenated analog of AEA, *N*-arachidonoyl glycine (NA-Gly), was synthesized as part of a structure-activity relationship (SAR) study of AEA (Burstein et al., 1997; Sheskin et al., 1997) and shown to suppress pain induced by thermal and chemical stimuli in rodents (Burstein et al., 1997; Huang et al., 2001). NAGly was subsequently identified as an endogenous lipid in the mammalian nervous system (Huang et al., 2001) and found to be a high-affinity ligand for the orphan GPCR GPR18 (Kohno et al., 2006).

Although the subfamily of arachidonoyl amides has received considerable attention, much less is known about the presence and activity of their saturated counterparts (Bradshaw and Walker, 2005). The most studied member of the saturated acyl amides is *N*-palmitoyl ethanolamine (PEA), an endogenous lipid with anti-inflammatory properties recently identified as an activator of the peroxisome proliferator-activated receptor and the orphan receptor GPR55 (Lo Verme et al., 2005; Ryberg et al., 2007). These findings highlight the growing number of bioactive *N*-acyl amides, a novel family of putative endogenous signaling lipids with multiple effects on pain, inflammation, and other biological systems.

Several pathways for the formation of *N*-acyl glycines were described, including 1) production via the enzyme glycine *N*-acylase found in the mitochondria of bovine liver and shown active with a variety of acyl-CoA donors, including aliphatic short and medium chains (2–10 carbons) and aromatic acyl thioesters (Schachter and Taggart, 1954). 2) The enzyme bile acid CoA:amino acid *N*-acyl transferase found in microsomes and peroxisomes and shown to conjugate bile acids mainly to glycine and taurine (O'Byrne et al., 2003). Bile acid CoA:amino acid *N*-acyl transferase was also shown to conjugate saturated 16- to 20-carbon fatty acids to glycine in vitro but with only 20% of the activity reported for bile acids. 3) Cytochrome *c*, acting with hydrogen peroxide as a cofactor, produced *N*-oleoyl glycine and NAGly in vitro when incubated with glycine and the respective fatty acid CoA (Mueller and Driscoll, 2007; McCue et al., 2008). 4) Oxygenation of *N*-acyl ethanolamines via the sequential enzymatic reaction of an alcohol dehydrogenase and aldehyde dehydrogenase (Burstein et al., 2000; Bradshaw et al., 2006a). Based on the presence of the potent anti-inflammatory lipid signaling molecules PEA and NAGly, and the presence of

several glycine-conjugating enzymes, we predicated the endogenous production of *N*-palmitoyl glycine (PalGly) as a putative signaling molecule.

Using partially purified lipid extracts from rat brain, we identified PalGly by nano-high-performance liquid chromatography (HPLC) quadrupole time-of-flight (QqTOF) mass spectrometry. By means of HPLC/MS/MS, we determined that the levels of PalGly were 3-fold greater in brain and 100-fold greater in skin compared with those reported for the endocannabinoid AEA (Felder et al., 1996; Bradshaw et al., 2006b). To determine whether PalGly was metabolically regulated by fatty acid amide hydrolase (FAAH), we measured its levels in the brain of FAAH knockout (KO) mice and found them to be significantly higher in KO compared with wildtype (WT) animals. We hypothesized that PalGly may act as a signaling molecule in dorsal root ganglion (DRG) cells based upon the high levels in skin and spinal cord and its structural similarities to endocannabinoids and PEA, which produce antinociceptive and anti-inflammatory effects. Electrophysiological studies in intact animals showed that a submicrogram dose of PalGly administered subdermally in the paw of a rat potently inhibited heat-evoked firing of nociceptive dorsal horn wide dynamic range (WDR) neurons. Using a DRG-like cell line, F-11, we revealed that PalGly induces transient influx of calcium followed by nitric oxide production via calcium-sensitive nitric-oxide synthase enzymes. PalGly likewise produced calcium influx in native adult DRG cells.

Materials and Methods

Chemicals.

HPLC grade water, methanol, and acetonitrile used for mass spectrometric studies were purchased from VWR International (Plainview, NY). Mass spectrometry/HPLC grade acetic acid, formic acid, and ammonium acetate were purchased from Sigma-Aldrich (St. Louis, MO). NAGly, [$^2H_8$]-NAGly, and *N*-linoleoyl glycine (LinGly) were purchased from Cayman Chemical (Ann Arbor, MI). Fatty acids were purchased from Nu-Chek Prep (Elysian, MN). URB597, SK&F96365, ω-conotoxin MVIIC, and ω-conotoxin GVIA were purchased from BIOMOL Research Laboratories (Plymouth Meeting, PA). Glycine, thapsigargin, ruthenium red, 4-phenyl-3-butenoic acid, and PTX were purchased from Sigma-Aldrich. SR144528 and SR141716A were a gift from sanofi-aventis (Montpellier, France). Fura-2 AM was purchased from Invitrogen (Carlsbad, CA). 5′-Iodoresiniferatoxin (I-RTX) and MK801 maleate were purchased from Tocris Cookson Inc. (Ellisville, MO) and LC Laboratories (Woburn, MA). The synthesis of *N*-acyl amino acid standards is detailed in Supplemental Data.

Antibodies.

Antibodies of mouse nNOS were purchased from BD Biosciences Transduction Laboratories (San Diego, CA). Antibodies of rabbit eNOS and iNOS were purchased from Abcam Inc. (Cambridge, MA). Rabbit anti-p38 MAPK antibody and mouse anti-phospho-p38 MAPK antibody were both purchased from Cell Signaling Technologies Inc. (Danvers, MA).

Animals.

Adult male and female Sprague-Dawley (Harlan, Indianapolis, IN) rats were used. All protocols were approved by the Indiana University Institutional Animal Care and Use Committee. Six male (300–450 g) and six female (250–300 g) Sprague-Dawley rats were used to conduct these studies. The FAAH WT and KO mice used in this study were littermates from the 13th generation offspring from intercrosses of 129SvJ-C57BL/6 FAAH KO and WT mice (Cravatt et al., 2001). In brief, the generation of FAAH KO mice was achieved by isolating the FAAH gene from a 129SvJ genomic library first, and a 2.5-kb region encompassing the first exon was mapped and sequenced. The first FAAH exon (encoding amino acids 1–65) and ≈2 kb of an upstream sequence were then replaced by inserting a PGK-Neo cassette between EcoRI and EcoRV sites located 2.3 kb apart. Homologous recombinant 129SvJ embryonic stem cell clones were identified by Southern analysis, and two clones were used to generate chimeric mice on a C57BL/6 background. Chimeras from both clones gave germline transmission of the mutated gene.

Partial Purification of PalGly from Mammalian Tissues.

Six fresh male rat brains were homogenized in the methanol fraction of 20 volumes to weight of 2:1 chloroform/methanol and centrifuged for 15 min at 31,000*g* at 24°C. Chloroform and NaCl (0.2 volume, 0.73%) were added to the supernatant, and the solution was centrifuged at 1000*g* for 15 min. The upper phase was discarded, and the interphase was washed twice. The lower phase was applied to diethylaminopropyl silica-based solid-phase extraction columns (Varian, Harbor City, CA) without prior column conditioning. The columns were sequentially washed with chloroform, methanol, and 0.1% ammonium acetate in methanol and eluted with 0.5% ammonium acetate in methanol. HPLC grade water (2.3 vol) was added to the eluate, and the solution was loaded onto preconditioned C-18 Bond-Elut 500-mg solid phase extraction columns (Varian). The cartridges were washed with water and 60% methanol and eluted with 80% methanol. Samples were evaporated in a SpeedVac (Thermo Fisher Scientific, Waltham, MA), reconstituted in 1 ml of chloroform, and applied to a 100-mg silica column (Bond-Elut SI; Varian) with no preconditioning. The column was washed with chloroform and 10% (v/v) methanol in chloroform, and eluted with 25% (v/v) methanol in chloroform. The eluate was evaporated in a SpeedVac, reconstituted in acetonitrile, and diluted to 2:1 HPLC grade water/acetonitrile before analysis.

Nano-HPLC Quadrupole-TOF Analysis of PalGly.

Exact mass measurements and structural characterization of PalGly from rat brain extract were performed with a hybrid QqTOF mass spectrometer (QSTAR Pulsar; Applied Biosystems/MDS Sciex, Foster City, CA). Extracts were chromatographed on a nano-HPLC C18 column (100 mm × 75 μm) coupled to a gradient nano-HPLC pump (Micro-Tech Scientific Inc., Vista, CA) operating at a flow rate of 300 nl/min. Chromatographic gradients began with 30% mobile phase B (98% acetonitrile, 0.1% formic acid):70% mobile phase A (2% acetonitrile, 0.1% formic acid) held for 10 min during sample loading, followed by a linear gradient from 30% B to 100% B over 30 min and then held at 100% B for 30 min. The electrospray ionization voltage was +3000 V, generating positively charged $[M+H]^+$ molecular and fragment ions.

Quantification of Tissue Levels of PalGly.

PalGly was extracted and quantified using methods similar to those developed and reported previously by this laboratory for extraction of NAGly (Huang et al., 2001; Bradshaw et al., 2006b). In brief, each tissue sample was subjected to a methanol extraction and partially purified using C18 solid phase extraction columns (Varian), with a final elution of 100% methanol. Rapid separation of analytes was obtained using 10-μl injections of analyte (Agilent 1100 series autosampler; Agilent Technologies, Wilmington, DE) onto a Zorbax eclipse XDB 2.1- × 50-mm reversed phase column. Gradient elution (200 μl/min) was formed under pressure on a pair of Shimadzu (Columbia, Maryland) 10AdVP pumps. Mass spectrometric analysis was performed with an Applied Biosystems/MDS Sciex API 3000 triple quadrupole mass spectrometer equipped with a heat-assisted electrospray ionization source. The MRM analyses used for quantification of tissue levels were conducted in negative ion mode with parent and fragment ions as follows: PalGly 312.2→74.2 and [$^2H_8$]NAGly 368.2→76.2. [$^2H_8$]NAGly was used as an internal standard to calculate recovery. The percentage of analyte recovered based upon the internal standard was 73.4 ± 0.16 (mean percentage ± S.E.).

Analysis of Brain Extracts from FAAH KO and WT Mice.

FAAH KO and WT mice were sacrificed when they were 6 weeks old. The brains were dissected and stored at −80°C until used. Lipid extraction, partial purification, and quantitation were performed as described above.

Effects of Inhibition of FAAH and PAM on Brain Levels of *N*-Palmitoyl Glycine.

Rats were injected with the FAAH inhibitor URB597 [3 mg/kg i.p. in 1% dimethylsulfoxide (DMSO) in saline], the peptidylglycine α-amidating monooxygenase (PAM) inhibitor 4-phenyl-3-butenoic acid (250 mg/kg i.p. in saline adjusted to pH 7.4 with sodium hydroxide), or the appropriate vehicle. Two hours later, the rats were decapitated, and brains were dissected and flash-frozen in liquid nitrogen, extracted, purified, and analyzed as described above.

Electrophysiological Recordings from Spinal Dorsal Horn.

Procedures for determination of the recording site in the dorsal horn, general electrophysiological methods, determination of the receptive field, assessment of heat-evoked firing rates, and data analysis were performed as reported by Huang and Walker (2006). In brief, neurons were classified as WDR nociceptive neurons if they exhibited increasing firing rates to application of increasing intensity of stimulation (brush, pressure, pinch, and heat) to the hind-paw skin. After identification of a WDR neuron, heat-evoked responses were elicited using a computerized apparatus that applied increasing intensities of radiant heat to the receptive field on the plantar surface of the paw over a 30-s interval. After the establishment of stable baseline responses (3 trials at 10-min intervals), PalGly (0.43 μg; n = 4) or vehicle (1:1:18, ethanol/Emulphor/saline; n = 5) was injected into the receptive field of the neuron (hind paw) in a volume of 50 μl, and heat-evoked responses were measured again. Postdrug heat-evoked responses were assessed at 10-min intervals for 30

min. Data from the three trials at 10, 20, and 30 min were analyzed as postinjection responses and the three trials conducted before injection as baseline responses.

Cell Culture.

The F-11 cell line (rat dorsal root ganglion neuron × mouse neuroblastoma) was provided by Dr. Mark C. Fishman (Massachusetts General Hospital, Boston, MA). F-11 cells were cultured in Ham's F-12 medium (1×) with L-glutamine (Mediatech, Herndon, VA) containing 1% penicillin-streptomycin (Invitrogen), 2% liquid mixture of sodium hypoxanthine/aminopterin/thymidine supplement (50×; Invitrogen), and 17% fetal bovine serum (FBS; Omega Scientific, Tarzana, CA). Cells were subcultured every other day using nonenzymatic cell dissociation solution (Sigma-Aldrich). Cells were grown under 5% CO_2 at 37°C. Native adult DRG cells were harvested from 175- to 200-g male rats as described in detail by Burkey et al. (2004). Cells were grown in adult growth medium containing: Ham's F-12 medium with nerve growth factor (30 ng/ml), normocin O (100 μg/ml; Invitrogen), 2 mM L-glutamine (Invitrogen), 1% penicillin-streptomycin (50 U/ml and 50 μg/ml; Invitrogen), 10% horse serum, and the mitotic inhibitors 5-flouro-2′-deoxyuridine (50 μM; Sigma-Aldrich) and uridine (150 μM; Sigma-Aldrich). The HEK293 cells stably transfected with human TRPV1 were a kind gift from Merck (Whitehouse Station, NJ). The HEK 293 TRPV1 cell line was cultured in minimal essential medium, Eagle, modified with nonessential amino acids, 1 mM sodium pyruvate, 2 mM L-glutamine, and 1.5 g/l sodium bicarbonate (American Type Culture Collection, Manassas, VA), containing 1% penicillin-streptomycin and 10% FBS. The mouse TRPV3-YFP, rat TRPV4, and mock-transfected pcDNA3 HEK293 cell lines were a kind gift from Dr. Michael J Caterina of Johns Hopkins University. These cells were cultured in DMEM 1X with L-glutamine (Mediatech), containing 1% penicillin-streptomycin (Invitrogen) and 10% FBS. All HEK293 cells were passaged three times a week using 0.25% trypsin-EDTA 1 (Invitrogen) and grown under 5% CO_2 at 37°C.

Effects of Neuron Depolarization on PalGly Levels in F-11 Cells.

F-11 cells were plated in 10-cm plates (650,000 cells/plate) 24 h before stimulation. Cells were washed three times with Hanks' balanced salt solution (Invitrogen) and incubated for 10 min at room temperature with 5 ml of Ham's F-12 medium (without FBS or antibiotics) containing 65 mM KCl or vehicle. The stimulated cells were collected, methanol extracts were partially purified on 500 mg of C8 solid phase extraction columns, and PalGly levels were quantified using MRM on a triple quadrupole mass spectrometer as described above. The experiment was repeated three times. In one experiment, the media were changed 10 min after treating cells with KCl as described above, and the cells were examined the following day, which revealed that the cells recovered from treatment with KCl.

Measurement of Ca^{2+} Influx in F-11 Cells and Transfected HEK293 Cells.

The calcium-sensitive fluorophore Fura-2 was used to measure intracellular calcium in F-11 cells using both single cell imaging and high-throughput 96-well plate assays. For single cell imaging, F-11 cells were plated on poly-D-lysine- or collagen-coated glass coverslips 24 h before imaging. Immediately before imaging, cells were loaded with 3 μM Fura-2 AM in Ham's F-12 medium (1×) with L-glutamine for 60 min at room temperature. Cells were then

washed three times with Ham's F-12 medium and mounted onto an inverted microscope (TS-100; Nikon, Tokyo, Japan). Test compounds were added to the cells after 60-s baseline recording. During recording, cells were alternately excited at 340 and 380 nm by switching optical filters mounted in a computer controlled Sutter wheel (Sutter Instrument Company, Novato, CA) using a xenon arc illuminator. Excitation light was reflected from a dichroic mirror through a 20× plan fluor objective. Light emitted at an emission wavelength of 510 nm was projected onto a Cohu 4920 cooled charge-coupled device camera (Cohu, San Diego, CA), and intracellular Ca^{2+} concentrations were analyzed with the InCyt Im2 image acquisition and analysis software (Intracellular Imaging Inc., Cincinnati, OH). The system was calibrated using a Fura-2 calibration kit (Invitrogen). Data were quantified by integrating the area under calcium concentration (nanomolar) time × (seconds) curves. Stably transfected HEK293 cells expressing TRPV3, TRPV4, and human-TRPV1 were imaged under the same conditions except that all procedures were carried out in HEPES-Tyrode buffer. The reagents 2-aminoethoxydiphenyl borate (Calbiochem/EMD Biosciences, San Diego, CA), 4α-phorbol-12,13-didecanoate (PKC Pharmaceuticals, Woburn, MA) and capsaicin (Sigma-Aldrich) were used as positive controls for TRPV3-, TRPV4-, and human-TRPV1-expressing cells, respectively.

For high-throughput assays, F-11 cells were plated on CellBIND 96-well flat clear-bottomed black polystyrene microplates (Corning Life Sciences, Acton, MA) 24 h before imaging. Cells were then loaded for 60 min at room temperature with 3 μM Fura-2 AM in Ham's F-12 medium (1×) with L-glutamine containing 0.05% (w/v) Pluronic F-127 (Invitrogen) and washed twice with Ham's F-12 medium (1×) with L-glutamine. The 340/380 fluorescence ratio was recorded for each well using a FlexStation II (Molecular Devices, Sunnyvale, CA). Data were quantified by integrating the area under 380/340 fluorescence ratio × time (seconds) curves.

The following conditions were used for drug administration: ruthenium red, glycine, MK801, SK&F96365, and ω-conotoxins were dissolved in H_2O; all other compounds were dissolved in DMSO. The final concentration of DMSO was less than 2% in all experiments (up to 2% DMSO did not affect calcium mobilization). To examine the effects of intracellular calcium store depletion, cells were pretreated and imaged with 500 nM thapsigargin, a Ca^2-ATPase inhibitor. As expected, thapsigargin produced intracellular calcium release followed by a gradual return to baseline. After baseline levels were reestablished, cells were treated with PalGly. To test the effects of glutamate, cannabinoid receptor antagonists and ω-conotoxins, cells were treated with MK801 (24 μM), SR144528 (150 nM), SR141716A (150 nM), or ω-conotoxins (2 μM) for 20 min before PalGly administration. The effects of SK&F96365 (10 or 25 μM) and ruthenium red (10 μM) were examined by applying these compounds onto cells immediately before imaging. For assays testing dependence on extracellular calcium, Fura-2-loaded cells were imaged in a HEPES-Tyrode's solution with or without calcium ions, pH 7.4. To test the effects of pertussis toxin, cells were incubated overnight with PTX (250 or 500 ng/ml) before the administration of PalGly.

Single-Cell Measurement of Ca^{2+} Influx in Native DRG Cells.

Native adult DRG cells were plated on poly-D-lysine- (Sigma-Aldrich) and laminin (Sigma-Aldrich)-coated glass coverslips in adult growth medium. Fura-2 was used to measure changes in intracellular calcium. Before imaging, cells were loaded with 3 μM Fura-2 AM in Ham's F-12 medium (1×) with L-glutamine (no other supplements were added) for 60 min at room temperature. Cells were then washed three times with Ham's F-12 medium with L-glutamine and mounted onto the inverted microscope as described previously. To identify the neuronal cells for imaging, we identified and circled the cells under bright field conditions. We chose the cells with typical DRG rounded morphology, as shown by Burkey et al. (2004). Test compounds (16 μM PalGly or vehicle) were manually added to the cells after 60-s baseline recording. At 400 s, after a brief wash, capsaicin (50 nM) was applied to the DRG cells and was used as a positive control in vehicle- or PalGly-treated cells.

P38 MAPK in Cell Western Assay.

F-11 cells were plated at 80% confluence and treated with PalGly (10 nM–20 μM). Upon completion of the PalGly treatment, an in-cell Western assay was conducted by the following procedure: the media were removed, and the cells were immediately fixed with a solution of 3.7% formaldehyde in PBS for 20 min at 20°C. The cells were then washed with a solution of 0.1% Triton X-100 in PBS with moderate shaking for 5 min at 20°C, the wash solution was removed and washed four more times. After the final wash, the cells were blocked with Odyssey blocking buffer (Cell Signaling Technologies Inc.) with moderate shaking for 90 min at 20°C. Primary antibodies anti-p38 and antiphospho-38 were diluted in Odyssey blocking buffer 1:200. For all PalGly concentrations tested, the Odyssey blocking buffer was removed from the relevant wells in the plate and replaced with buffer containing primary antibodies, whereas again for each concentration tested corresponding control wells received no primary antibody. The plate was then incubated overnight with moderate shaking at 4°C. After incubation with the primary antibody, the wells were then washed five times with PBS/0.1% Tween 20 for 5 min at 20°C. Fluorescently labeled antibodies (Odyssey goat anti-rabbit 680-nm antibody and goat anti-mouse 800-nm antibody) were diluted in Odyssey blocking buffer 1:800 containing 0.2% Tween 20; secondary antibody solution was added to all wells and incubated in the dark for 1 h at 20°C. The wells were then washed five times with PBS/0.1% Tween 20 for 5 min at 20°C. The plate was then scanned using the Odyssey Infrared Imaging System (Li-Cor, Lincoln, NE), using both 700- and 800-nm channels, a resolution of 169 μm, an intensity of 5, and focal offset of 4 mm. Changes in p38 MAPK were then determined by calculating the mean background fluorescence from all nonprimary antibody containing control wells, for both 700- and 800-nm channels. Background fluorescence was then subtracted from the fluorescence measured in primary antibody containing PalGly wells, for both p38 MAPK and phospho-p38 MAPK. The changes in p38 MAPK phosphorylation were then obtained by constructing the ratio of p38:phospho-p38 MAPK fluorescence for all concentrations of PalGly tested.

Western Blotting.

Western blotting was carried out as described previously (Rimmerman et al., 2008) and optimized for the detection of phosphorylated proteins according to Prieto et al. (2007) by

supplementing the lysis buffer with phosphatase inhibitor cocktails (type I and II; Sigma-Aldrich) in concentrations suggested by the manufacturer. The blocking buffer consisted of Tris-buffered saline/Tween 20 (10 mM Tris-HCl, pH 7.5, 150 mM NaCl, and 0.1% Tween 20) containing 3% skim milk (Carnation; Nestle, Vevey, Switzerland) to detect nonphosphorylated proteins, or the blocking buffer consisted of Tris-buffered saline/Tween 20 containing 1% bovine serum albumin (Fisher Scientific, Pittsburgh, PA) and 10 mM NaF, 2 mM Na_3VO_4, and 5 mM $Na_4P_2O_7$ to detect phosphorylated proteins. The membranes were incubated overnight at 4°C in the presence of primary antibody. The following antibodies were used for the Western blot analyses: anti-nNOS (155 kDa; 1:2500 dilution), anti-phospho (Ser847) nNOS (160 kDa; 1:1000 dilution), anti-eNOS (133 kDa; 1:1000 dilution), anti-iNOS (131 kDa; 1:500–1000 dilution).

Nitric Oxide Imaging.

Nitric oxide production in F-11 cells was measured using the nitric oxide sensing fluorophore DAF-2 (Cayman Chemical). In brief, F-11 cells were plated on 96-well plates (Cell-BIND; Corning Life Sciences) and grown overnight before experiments. Cells were incubated for 1 h in serum-free Ham's F-12 containing 5 μM DAF-2 DA and 0.002% Pluronic F-127 (Invitrogen). At the end of the incubation period, cells were washed once using Ham's F-12 medium, which was also used as the recording medium. Fluorescence (excitation, 485 nm; emission, 530 nm) was recorded from each well for 240 s using a Flexstation II (Molecular Devices). Automated additions of drug occurred after 20-s baseline recordings. All drugs were initially dissolved in DMSO and diluted in recording medium to a final DMSO concentration of 1%. To test the effects of the calcium entry blocker SK&F96365 (BIOMOL Research Laboratories), cells were loaded with DAF-2 as mentioned above and washed twice, followed by addition of the recording medium. SK&F96365 (28.6 μM) or the vehicle (water; 1.4%) was added to the wells followed immediately by data acquisition, during which drug additions lowered these concentrations to their final values of 20 μM SK&F96365, with a vehicle concentration of 1%. For experiments with the NOS inhibitor 7-nitroindazole (7-NI; Sigma-Aldrich), serum-free F-12 medium preparations were made containing either 200 μM 7-NI or the vehicle DMSO (0.2%). Cells were first incubated for 3.25 h at 37°C in Ham's F-12 medium containing either 7-NI or DMSO, after which loading, washing, and recording were conducted as described above but using the Ham's F-12 medium containing 7-NI or DMSO. Data from cell-based assays were normalized to the effect of the NO donor *S*-nitroso-*N*-acetyl-DL-penicillamine (SNAP) on DAF-2 fluorescence in cell-free assays. Fluorescence was measured in cell-free wells containing 5 μM DAF-2 (Cayman Chemical) to which 2 mM SNAP or vehicle (DMSO; 1%) was added.

To ensure that pretreatment with 7-NI did not cause cell death, cell viability was measured using trypan blue (Sigma-Aldrich). Cells were treated with 7-NI or DMSO exactly as for the fluorescence assays. However, after loading and washing, the cells were treated for 5 min with 0.2% trypan blue in Ham's F-12 medium. The percentage of viable cells was calculated by examining random fields of view in the 7-NI and DMSO treatment conditions.

Data Analysis.

Results were analyzed using one-way ANOVA with Fisher's LSD, Bonferroni Dunnett post hoc tests, or Student's *t* test depending on the type of comparison. Data are presented as means ± S.E.M.; $p < 0.05$ was considered statistically significant. Calcium data from single cell recording were analyzed using cubic spline interpolation (MATLAB, 2004; Mathworks Inc., Natick, MA). For each cell, data were normalized by estimating the baseline level of calcium and subtracting it from the post-treatment levels. Data from the DAF-2 fluorescence assays were analyzed using SoftMax Pro version 4.8 (Molecular Devices). Data points were expressed as a percentage of baseline fluorescence and area under the curve (AUC) was computed for each well. Drug effects were assessed as the AUC of drug treatment minus the AUC of vehicle.

Results

Isolation, Identification, and Tissue Distribution of PalGly

Methanol extracts of rodent brain were analyzed by mass spectrometry in a search for the 16-carbon saturated fatty acid conjugated to a glycine molecule through an amide bond, PalGly (Fig. 1A). By comparing the extracted analyte to the synthetic PalGly standard using LC/MS/MS, we found that both had matching mass spectra and retention times (Fig. 1, B–D). Exact mass measurements and product ion scans with nano-HPLC/qQTOF permitted further characterization of the extracted lipid (Fig. 1, F and G). The mass of the molecular ion of each compound in the extract deviated from that of the theoretical exact mass of PalGly by <5 ppm, and fragment ions differed from the theoretically predicted ions by no more than 16 ppm (Fig. 1H). Based on the matching HPLC retention times, mass spectra, and exact masses of the tissue-derived analyte and synthetic standard, we can conclude that PalGly is a naturally occurring constituent of mammalian tissues.

PalGly Is Produced after Neuronal Depolarization and Is Metabolized by FAAH

In light of observations indicating that signaling lipids such as the endocannabinoids AEA and 2-arachidonoyl glycerol (2-AG) are made on demand in response to cellular stimulation (Di Marzo et al., 1999), we hypothesized that PalGly could be produced under similar conditions. We incubated the DRG-like cell line (F-11) with depolarizing media containing 65 mM KCl for 10 min. Quantification of the levels of PalGly revealed a significant increase (25.3%) in the KCl-stimulated cells over the unstimulated cells (unstimulated cells 335.0 ± 43.3 fmol/1 × 10^6 cells versus stimulated cells 419 ± 9.34 fmol/1 × 10^6 cells; $p < 0.05$.)

FAAH and PAM are enzymes known to metabolize other acyl amides such as AEA, oleamide, and the *N*-acyl taurines (Ritenour-Rodgers et al., 2000; McKinney and Cravatt, 2005). Therefore, we hypothesized that either FAAH or PAM would act on PalGly. Although the PAM inhibitor 4-phenyl-3-butenoic acid failed to alter brain levels of PalGly, 3 mg/kg FAAH inhibitor URB597 nearly doubled the levels of PalGly in brain compared with vehicle (DMSO, 47.51 ± 6.56 pmol/g; URB597, 90.41 ± 5.84 pmol/g; $p \leq 0.05$). Consistent with this observation, the levels of PalGly were markedly increased in the brains of FAAH KO mice compared with WT controls (WT, 26.2 ± 2.77 pmol/g; KO, 41.1 ± 3.63 pmol/g; $p \leq 0.05$).

PalGly Levels Are Highest in Skin, Lung, and Spinal Cord

The level of PalGly was quantified in methanol extracts of 12 tissues and organs by HPLC/MS/MS. PalGly was found in all tissues tested, although wide variations of its levels in the different tissues were observed (Fig. 1E). For example, the concentration of PalGly in skin was approximately 1600 pmol/g versus 50 pmol/g in brain. The levels of PalGly were approximately 3-fold greater in brain and 100-fold greater in skin compared with those of anandamide (Felder et al., 1996; Bradshaw et al., 2006b) and NAGly (Huang et al., 2001; Bradshaw et al., 2006b). However, comparable with the tissue distribution of NAGly (Huang et al., 2001), PalGly levels were highest in spinal cord, skin, and intestine, suggesting similarities in their biosynthetic pathways.

PalGly Modulates Heat-Evoked Responses of Dorsal Horn Wide Dynamic Range Neurons

Several acyl amides, including AEA, NAGly, and PEA, were reported to act as endogenous signaling lipids mediating antinociception (Bradshaw and Walker, 2005). Hence, the relatively high levels of PalGly in skin and spinal cord suggested a potential role of PalGly in the modulation of nociceptive pathways. To test this hypothesis, PalGly was administered intradermally to anesthetized rats, and single WDR neurons were selected for recording based on their increasing rate of firing in response to mechanical stimuli of increasing strength and their responses to noxious heat. Vehicle administration had no effect on neuronal firing compared with prevehicle responses. By contrast, intradermal administration of PalGly (0.43 μg in 50 μl of vehicle) in the receptive fields of these WDR neurons suppressed the responses to a heat stimulus at noxious temperatures (45–52°C; $p < 0.01$; Fig. 2) compared with pre-PalGly responses.

PalGly Induces Calcium Influx in DRG-like (F-11) Cells

To investigate the effect of PalGly on primary sensory neurons, calcium influx was recorded in the DRG-like F-11 cells. As shown in Fig. 3A, PalGly (10 μM) induced a transient influx of calcium in F-11 cells. The effect was immediate, and the initial increase was followed by a gradual return to baseline after 5 min of PalGly addition, with an EC_{50} = 5.5 μM (Hill slope = 4.7; R^2 = 0.99; Fig. 3B). Single cell calcium imaging further revealed a markedly lower level but still significant influx of calcium after application of *N*-stearoyl glycine and stearic acid (Fig. 4). However, other related molecules, including *N*-oleoyl glycine, LinGly, NAGly, *N*-docosahexaenoyl glycine, and free glycine were inactive at concentrations up to 50 μM (Fig. 4). Palmitic acid and *N*-palmitoyl L-alanine also failed to alter calcium influx at concentrations up to 25 and 50 μM, respectively, demonstrating strict structural requirements for both the lipid and polar moieties of PalGly (Fig. 4). To test the possibility that the effects of PalGly were mediated by a GPCR linked to a PTX-sensitive G subunit, F-11 cells were incubated overnight with PTX (250 or 500 ng/ml). The effect of PalGly was significantly reduced after PTX treatment but not abolished (Fig. 5). Treatment with the specific P/Q or N-type voltage-gated calcium channel blockers ω-conotoxin MVIIC or ω-conotoxin GVIA, did not block calcium influx (2 μM; Fig. 5). To determine the source of calcium influx, experiments were performed in the presence or absence of extracellular calcium and in cells treated with thapsigargin (500 nM) or cyclopiazonic acid (37 μM) to deplete intracellular stores. Calcium influx by PalGly was dependent on the presence of extracellular calcium

[$t(146) = 9.4$; two-tailed, $p < 0.001$] and was not reduced after treatment with thapsigargin (500 nM) or cyclopiazonic acid (37 μM).

F-11 cells express several lipid-activated receptors such as CB_1 and CB_2 (Ross et al., 2001) as well as several TRPV subtypes (Jahnel et al., 2003), each of which regulates calcium levels. The CB_1 antagonist SR141716A (150 nM) and the CB_2 antagonist SR144528 (150 nM) failed to inhibit PalGly-induced calcium influx. The *N*-methyl-D-aspartate channel blocker MK801 (25 μM), and the TRPV1-specific blocker I-RTX (35 nM) also failed to block PalGly-induced calcium influx (Fig. 6D). By contrast, the nonspecific calcium channel blockers ruthenium red (10 μM) and La^{3+} (1 mM) blocked the influx of calcium produced by PalGly (Fig. 6, A, B, and D). In addition, the receptor or store-operated calcium channel inhibitor SK&F96365 significantly attenuated the effects of PalGly in a dose-dependent manner (Fig. 6, C and D). PalGly had no effect on p38 MAPK phosphorylation in F-11 cells and did not induce calcium influx in HEK293 cells stably expressing mouse-TRPV3-YFP, rat-TRPV4, or human-TRPV1 (Supplemental Data).

PalGly Dose-Dependently Increases Nitric Oxide Production in Vitro

NO inhibited neuronal firing in several sensory systems (Chaban et al., 2001; Clasadonte et al., 2008), and both calcium-dependent nitric-oxide synthase (NOS) isoforms (neuronal and endothelial) were detected in F-11 cells (Fig. 7A) (Rimmerman et al., 2008). Therefore, we hypothesized that the reduction in firing rate of the WDR cells in response to PalGly seen in vivo may be mediated through the activation of calcium-sensitive NOS enzymes and production of NO. NO production was monitored using the fluorescence dye DAF-2. We observed that PalGly but not other *N*-acyl glycines induced NO production in a dose-dependent manner (Fig. 7, D and E). NO production was blocked by the nonselective calcium channel blocker SK&F96365 [Fig. 7B; $t(10) = -2.3$, two-tailed, $p < 0.05$] and was attenuated by the NOS blocker 7-NI (Fig. 7F). 7-NI treatment did not affect cell viability, tested using trypan blue as mentioned under Materials and Methods. The time course for calcium influx and NO production is shown in Fig. 7C by the overlay of a single cell calcium and a single cell NO trace (Fig. 7C).

PalGly Induces Calcium Influx in Native DRG Cells

PalGly Induces Calcium Influx in Native DRG Cells.—Finally, we asked whether PalGly would cause similar influx of calcium in primary adult rat DRG cells. We tested native adult DRG cells 24 to 48 h after plating. We found that PalGly produced a transient calcium influx with a rapid return to baseline (Fig. 8A) in a manner that paralleled that observed with F-11 cells. Capsaicin (50 nM) was used as a positive control. Fifteen of 34 (44%) of the DRG cells that were treated with PalGly (16 μM) responded with an average increase ≥50 nM above baseline (calculated across 60 s after application). The average increase in calcium influx after PalGly application was significantly different from the average increase after vehicle treatment (Fig. 8B).

Discussion

Based on the presence of glycine-conjugating enzymes and saturated bioactive lipid conjugates such as PEA, we hypothesized the presence and bioactivity of PalGly in mammalian tissues. We found a significant rise (~25%) in the levels of PalGly after KCl-induced depolarization of F-11 cells. In addition, PalGly was identified as an endogenous molecule in rat tissues under basal conditions, and its levels were modulated by knockout of the gene for the lipid-metabolizing enzyme FAAH in vivo. Huang et al. (2001) reported previously that NAGly, and less so PalGly and LinGly, inhibited the hydrolysis of anandamide by FAAH in vitro. These findings led us to investigate the potential role of PalGly as a biological mediator.

The high basal levels of PalGly found in rat skin and spinal cord were suggestive of its involvement in cutaneous signaling. Cutaneous signaling through peripheral receptors activated by lipid molecules (including TRP channels and GPCRs) modulates the firing rate of stimulated WDR neurons (Elmes et al., 2004; Huang et al., 2006; Merrill et al., 2008). We used this in vivo model to determine whether peripherally administered low doses of PalGly would produce upstream effects on heat-stimulated WDR neurons. Indeed, we discovered that a submicrogram dose of PalGly (0.43 μg in 50 μl) significantly suppressed heat-evoked responses of WDR neurons when the heat stimulus increased the temperature of the rat paw to above 43°C.

WDR neurons receive innervations from peripheral C and A fibers that encode both noxious and innocuous stimuli and project to higher brain centers; therefore, inhibitory effects on these neurons can modulate upstream sensory processing (Elmes et al., 2004; Willis, 2007). To shed light on the molecular components leading to this inhibitory effect, we used the hybrid DRG × neuroblastoma cell line (F-11) as a model system for studying the effects of PalGly on cell signaling. PalGly caused an immediate and robust calcium influx, with an EC_{50} value of 5.5 μM. This level is similar to the endogenous concentration measured in skin under basal conditions, ~1.6 μM. Given that the amount reported here in the skin was averaged across the entire dissected tissue, it likely underestimates the local concentrations of this lipophilic molecule in specific cellular compartments. For example, we demonstrated previously that 2-AG clusters within lipid rafts (Rimmerman et al., 2008). Tissue levels of PalGly also do not account for the heterogeneity of cell types, down-regulation of PalGly by FAAH or other enzymes, or up-regulation after cellular stimulation.

In vitro metabolism of PalGly was demonstrated previously using a bacterial cytochrome P450 (CYPBM-3). PalGly bound the enzyme with higher affinity than any other tested compound. The products of the enzymatic oxidation were ω−1, ω−2, and ω−3-monohydroxylated metabolites of PalGly (Haines et al., 2001). It is yet to be determined whether PalGly can bind mammalian cytochrome P450 enzymes in the same manner and whether these metabolites take part in the signaling mechanisms of this abundant lipid.

The structure-activity relationship study using six other *N*-acyl glycine molecules indicated strict structural requirements for PalGly signaling that were suggestive of receptor activation. In these experiments, the addition of a single methyl group to the polar moiety

(alanine versus glycine) led to a dramatic drop in activity, as did changes to chain length and degree of saturation in the lipid moiety. The influx of calcium by PalGly was inhibited by PTX (250–500 ng/ml), suggesting the involvement of a $G\alpha_{i/o}$-coupled signaling pathway. The effect of PalGly was also dependent on extracellular calcium. A similar pathway was described previously in the neuroblastoma × glioma hybrid cell line (NG108–15) after treatment with the endocannabinoid 2-AG. In contrast to 2-AG, the effect of PalGly was not inhibited by CB_1 and CB_2 antagonists. Moreover, PalGly-induced calcium influx was blocked by ruthenium red, La3+, and SK&F96365, which are nonselective antagonists of TRP channels and receptor-operated calcium channels (Merritt et al., 1990; Caterina et al., 1997).

Three pathways leading to cation influx through TRP receptor modulation have been described: ligand binding (e.g., Δ^9-tetrahydrocannabinol, *N*-arachidonoyl dopamine, anandamide, capsaicin, and diacylglycerol), direct activation (e.g., temperature, pH, osmolarity, and membrane stretch), and indirect activation through GPCR-mediated pathways (e.g., through phospholipase C, diacylglycerol production, and inositol 1,4,5-trisphosphate production; Ramsey et al., 2006). We ruled out simple ligand binding of PalGly to human-TRPV1, mouse-TRPV3, and rat-TRPV4 receptors by screening stably transfected HEK293 cells. The complex signaling properties of PalGly, including strict SAR, partial inhibition by PTX, and dependence on extracellular calcium, are suggestive of GPCR-mediated cation channel activation.

An analogous pathway involving the neuropeptide head activator, which drives cells into mitosis by its actions at GPR37, has been characterized previously (Rezgaoui et al., 2006). GPR37 activates a PTX-sensitive pathway regulating a TRPV-like calcium channel (the growth factor-regulated calcium-permeable cation channel) that could be inhibited by SK&F96365 (Boels et al., 2001). The influx of calcium induces the activation of acalcium-dependent K^+ channel, leading to cellular hyperpolarization. We are currently exploring whether a similar set of events is plausible for PalGly: activation of a PTX-sensitive GPCR followed by activation of a second messenger, which in turn modulates a TRP-like channel, promoting activation of a downstream channel leading to suppression of spinal circuits. Additional studies will investigate the role of PalGly on PPAR activation of calcium and as a ligand for GPR55 given the potent effects of the structural analog PEA in these systems.

The stimulation of nitric oxide production by PalGly is an additional downstream mechanism that could explain the heat-stimulated WDR neuronal firing inhibition produced by PalGly in vivo. The transient influx of calcium evoked by PalGly seems to activate calcium-dependent NOS enzymes present in F-11 cells, a conclusion based upon the failure of PalGly to induce production of NO in cells treated with the calcium channel blocker SK&F96365 and the similarity between the SARs of PalGly-induced calcium influx and NO production. The constitutive NOS isoforms generate relatively smaller NO fluxes with a shorter time course compared with inducible NOS (Wink and Mitchell, 1998). The effects of NO on neuronal firing differ among cell types, but several studies indicate that NO production leads to inhibition of neuronal firing and transmission (Chaban et al., 2001; Clasadonte et al., 2008). Hence, it is possible that the PalGly-induced NO production may contribute to the observed inhibition of heat-stimulated WDR neuronal firing in vivo. This

may occur via direct activation of soluble guanylate cyclase to produce cyclic GMP leading to protein kinase G activation and modulation of K^+ channels. This pathway was implicated in peripheral antinociceptive effects of several compounds, including indomethacin and dipyrone (Lorenzetti and Ferreira, 1996; Ventura-Martínez et al., 2004). Additional molecular studies testing cyclic GMP up-regulation and protein kinase G activation as well as physiological experiments using NOS inhibitors will be needed to test this hypothesis and investigate potential antinociceptive effects of PalGly.

In summary, we have provided mass spectrometric evidence for the novel endogenous lipid *N*-palmitoyl glycine that is produced throughout the body with the highest levels in skin and spinal cord, is hydrolyzed by FAAH, inhibits heat-evoked firing of WDR neurons, activates calcium influx in DRG cells and stimulates NO production. Together, these data provide a framework for further investigations into this putative signaling lipid and provide additional evidence into the investigations of a potentially larger family of acyl amide signaling lipids.

Supplementary Material

Refer to Web version on PubMed Central for supplementary material.

Acknowledgments

We thank Dr. Mika L. M. Macinnis (Brown University, Providence, RI) for creating the MATLAB program used to analyze calcium data. We dedicate this work to J.M.W. (1950-2008) whose love of science was an inspiration to all who worked with him.

This work was supported by National Institutes of Health/National Institute on Drug Abuse Grants DA16825 and DA018224, the Linda and Jack Gill Center for Biomolecular Science, Indiana University; a Faculty Research Support grant from Indiana University, Bloomington; and the MetaCyt Grant to Indiana University from the Lilly Foundation Inc., Indianapolis, IN. This work was part of the doctoral thesis of N.R. titled, *The Signaling Properties in Sensory Neurons of the Novel Endogenous Lipid N-Palmitoyl Glycine* (2007). This work was previously presented in the following symposia: Rimmerman N, Bradshaw HB, O'Dell DK, and Walker JM (2006) Cellular signaling properties of the newly identified fatty acid amide *N*-palmitoyl glycine found in rat central nervous system and skin in 16th Annual Symposium on the Cannabinoids, Burlington, VT, International Cannabinoid Research Society, p. 13; Hughes HV, Rimmerman N, Vasko MR, and Walker JM (2007) *N*-Palmitoyl glycine induces calcium mobilization in native dorsal root ganglion cells and nitric oxide production in F-11 cells expressing neuronal nitric oxide synthase. 17th Annual Symposium on the Cannabinoids, Burlington, VT, International Cannabinoid Research Society, p. 171; Bradshaw HB, Vefring E, Jahnsen JA, O'Dell KD, Burstein S, Walker JM (2005) Identification of novel brain-derived fatty acid amides in extracts of the rat brain. 15th Annual Symposium on the Cannabinoids, Burlington, VT, International Cannabinoid Research Society.

ABBREVIATIONS:

AEA	N-arachidonoyl ethanolamine (anandamide)
GPCR	G protein-coupled receptor
CB	cannabinoid
TRPV	transient receptor potential vanilloid
NAGly	N-arachidonoyl glycine
SAR	structure-activity relationship
PEA	N-palmitoyl ethanolamine

PalGly	N-palmitoyl glycine
HPLC	high-performance liquid chromatography
QqTOF	quadrupole time-of-flight
MS/MS	mass spectrometry
2-AG	2-arachidonoyl glycerol
FAAH	fatty acid amide hydrolase
KO	knockout
WT	wild type
DRG	dorsal root ganglion
WDR	wide dynamic range
LinGly	N-linoleoyl glycine
SK&F96365	1-(-[3-(4-methoxyphenyl)propoxy]-4-methoxyphenethyl)-1H-imidazole
PTX	pertussis toxin
SR141716A	N-(piperidin-1-yl)-5-(4-chlorophenyl)-1-(2,4-dichlorophenyl)-4-methyl-1H-pyrazole-3-carboximide hydrochloride
AM	acetoxymethyl ester
I-RTX	5-iodoresiniferatoxin
MK801	5H-dibenzo[a,d]cyclohepten-5,10-imine
URB597	cyclohexyl carbamic acid 3-carbamoylbiphenyl-3-yl ester
SR144528	N-(1,3,3-trimethylbicyclo(2.2.1)heptan-2-yl)-5-(4-chloro-3-methylphenyl)-1-(4-methylbenzyl)pyrazole-3-carboxamide
nNOS	neuronal nitric-oxide synthase
eNOS	endothelial nitric-oxide synthase
iNOS	inducible nitric-oxide synthase
MAPK	mitogen-activated protein kinase
kb	kilobase(s)
MRM	multiple reaction monitoring
PAM	peptidylglycine -amidating monooxygenase
DMSO	dimethyl sulfoxide

FBS	fetal bovine serum
HEK	human embryonic kidney
YFP	yellow fluorescent protein
PBS	phosphate-buffered saline
7-NI	7-nitroindazole
SNAP	S-nitroso-N-acetyl-DL-penicillamine
ANOVA	analysis of variance
LSD	least significant difference
LC	liquid chromatography
AUC	area under the curve
NOS	nitric oxide synthase
TRP	transient receptor potential
DAF-2	4,5-diaminofluorescein

References

Boels K, Glassmeier G, Herrmann D, Riedel IB, Hampe W, Kojima I, Schwarz JR, and Schaller HC (2001) The neuropeptide head activator induces activation and translocation of the growth-factor-regulated Ca^2-permeable channel GRC. J Cell Sci 114:3599–3606. [PubMed: 11707512]

Bradshaw HB and Walker JM (2005) The expanding field of cannabimimetic and related lipid mediators. Br J Pharmacol 144:459–465. [PubMed: 15655504]

Bradshaw HB, Hu SSJ, Rimmerman N, O'Dell DK, Masuda K, Cravatt BF, and Walker JM (2006a) Novel metabolism of NAGly by fatty acid amide hydrolase, in Proceedings of the 16th Annual Symposium on the Cannabinoids; 2006 June 24–28; Tihany, Hungary. p. 22, International Cannabinoid Research Society, Burlington, VT.

Bradshaw HB, Rimmerman N, Krey JF, and Walker JM (2006b) Sex and hormonal cycle differences in rat brain levels of pain-related cannabimimetic lipid mediators. Am J Physiol Regul Integr Comp Physiol 291:R349–R358. [PubMed: 16556899]

Burkey TH, Hingtgen CM, and Vasko MR (2004) Isolation and culture of sensory neurons from the dorsal-root ganglia of embryonic or adult rats. Methods Mol Med 99:189–202. [PubMed: 15131338]

Burstein SH, Pearson W, Rooney T, Yagen B, Zipkin R, and Zurier A (1997) Studies with analogs of anandamide and indomethacin, in Proceedings of the 7th Annual Symposium on the Cannabinoids; 1997 June 19–21; Stone Mountain, GA. p. 31. International Cannabinoid Research Society, Burlington, VT.

Burstein SH, Rossetti RG, Yagen B, and Zurier RB (2000) Oxidative metabolism of anandamide. Prostaglandins Other Lipid Mediat 61:29–41. [PubMed: 10785540]

Caterina MJ, Schumacher MA, Tominaga M, Rosen TA, Levine JD, and Julius D (1997) The capsaicin receptor: a heat-activated ion channel in the pain pathway. Nature 389:816–824. [PubMed: 9349813]

Chaban VV, McRoberts JA, Ennes HS, and Mayer EA (2001) Nitric oxide synthase inhibitors enhance mechanosensitive Ca^{2+} influx in cultured dorsal root ganglion neurons. Brain Res 903:74–85. [PubMed: 11382390]

Clasadonte J, Poulain P, Beauvillain JC, and Prevot V (2008) Activation of neuronal nitric oxide release inhibits spontaneous firing in adult gonadotropin-releasing hormone neurons: a possible local synchronizing signal. Endocrinology 149:587–596. [PubMed: 18006627]

Cravatt BF, Demarest K, Patricelli MP, Bracey MH, Giang DK, Martin BR, and Lichtman AH (2001) Supersensitivity to anandamide and enhanced endogenous cannabinoid signaling in mice lacking fatty acid amide hydrolase. Proc Natl Acad Sci U S A 98:9371–9376. [PubMed: 11470906]

Devane WA, Hanus L, Breuer A, Pertwee RG, Stevenson LA, Griffin G, Gibson D, Mandelbaum A, Etinger A, and Mechoulam R (1992) Isolation and structure of a brain constituent that binds to the cannabinoid receptor. Science 258:1946–1949. [PubMed: 1470919]

Di Marzo V, Bisogno T, and De Petrocellis L (2007) Endocannabinoids and related compounds: walking back and forth between plant natural products and animal physiology. Chem Biol 14:741–756. [PubMed: 17656311]

Di Marzo V, Bisogno T, De Petrocellis L, Melck D, Orlando P, Wagner JA, and Kunos G (1999) Biosynthesis and inactivation of the endocannabinoid 2-arachidonoylglycerol in circulating and tumoral macrophages. Eur J Biochem 264:258–267. [PubMed: 10447696]

Elmes SJ, Jhaveri MD, Smart D, Kendall DA, and Chapman V (2004) Cannabinoid CB2 receptor activation inhibits mechanically evoked responses of wide dynamic range dorsal horn neurons in naive rats and in rat models of inflammatory and neuropathic pain. Eur J Neurosci 20:2311–2320. [PubMed: 15525273]

Felder CC, Nielsen A, Briley EM, Palkovits M, Priller J, Axelrod J, Nguyen DN, Richardson JM, Riggin RM, Koppel GA, et al. (1996) Isolation and measurement of the endogenous cannabinoid receptor agonist, anandamide, in brain and peripheral tissues of human and rat. FEBS Lett 393:231–235. [PubMed: 8814296]

Haines DC, Tomchick DR, Machius M, and Peterson JA (2001) Pivotal role of water in the mechanism of P450BM-3. Biochemistry 40:13456–13465. [PubMed: 11695892]

Hohmann AG, Suplita RL, Bolton NM, Neely MH, Fegley D, Mangieri R, Krey JF, Walker JM, Holmes PV, Crystal JD, et al. (2005) An endocannabinoid mechanism for stress-induced analgesia. Nature 435:1108–1112. [PubMed: 15973410]

Huang SM, Bisogno T, Petros TJ, Chang SY, Zavitsanos PA, Zipkin RE, Sivakumar R, Coop A, Maeda DY, De Petrocellis L, et al. (2001) Identification of a new class of molecules, the arachidonyl amino acids, and characterization of one member that inhibits pain. J Biol Chem 276:42639–42644. [PubMed: 11518719]

Huang SM, Bisogno T, Trevisani M, Al-Hayani A, De Petrocellis L, Fezza F, Tognetto M, Petros TJ, Krey JF, Chu CJ, et al. (2002) An endogenous capsaicin-like substance with high potency at recombinant and native vanilloid VR1 receptors. Proc Natl Acad Sci U S A 99:8400–8405. [PubMed: 12060783]

Huang SM and Walker JM (2006) Enhancement of spontaneous and heat-evoked activity in spinal nociceptive neurons by the endovanilloid/endocannabinoid N-arachidonoyldopamine (NADA). J Neurophysiol 95:1207–1212. [PubMed: 16267120]

Jahnel R, Bender O, Munter LM, Dreger M, Gillen C, and Hucho F (2003) Dual expression of mouse and rat VRL-1 in the dorsal root ganglion derived cell line F-11 and biochemical analysis of VRL-1 after heterologous expression. Eur J Biochem 270:4264–4271. [PubMed: 14622291]

Kohno M, Hasegawa H, Inoue A, Muraoka M, Miyazaki T, Oka K, and Yasukawa M (2006) Identification of N-arachidonylglycine as the endogenous ligand for orphan G-protein-coupled receptor GPR18. Biochem Biophys Res Commun 347:827–832. [PubMed: 16844083]

Lo Verme J, Fu J, Astarita G, La Rana G, Russo R, Calignano A, and Piomelli D (2005) The nuclear receptor peroxisome proliferator-activated receptor-mediates the anti-inflammatory actions of palmitoylethanolamide. Mol Pharmacol 67:15–19. [PubMed: 15465922]

Lorenzetti BB and Ferreira SH (1996) Activation of the arginine-nitric oxide pathway in primary sensory neurons contributes to dipyrone-induced spinal and peripheral analgesia. Inflamm Res 45:308–311. [PubMed: 8814464]

McCue JM, Driscoll WJ, and Mueller GP (2008) Cytochrome c catalyzes the in vitro synthesis of arachidonoyl glycine. Biochem Biophys Res Commun 365:322–327. [PubMed: 17986381]

McKinney MK and Cravatt BF (2005) Structure and function of fatty acid amide hydrolase. Annu Rev Biochem 74:411–432. [PubMed: 15952893]

Merrill AW, Cuellar JM, Judd JH, Iodi Carstens M, and Carstens E (2008) Effects of TRPA1 agonists mustard oil and cinnamaldehyde on lumbar wide dynamic range neuronal responses to innocuous and noxious cutaneous stimuli in rats. J Neurophysiol 99:415–425. [PubMed: 17942619]

Merritt JE, Armstrong WP, Benham CD, Hallam TJ, Jacob R, Jaxa-Chamiec A, Leigh BK, McCarthy SA, Moores KE, and Rink TJ (1990) SK&F 96365, a novel inhibitor of receptor-mediated calcium entry. Biochem J 271:515–522. [PubMed: 2173565]

Milman G, Maor Y, Abu-Lafi S, Horowitz M, Gallily R, Batkai S, Mo FM, Offertaler L, Pacher P, Kunos G, et al. (2006) N-Arachidonoyl L-serine, an endocannabinoidlike brain constituent with vasodilatory properties. Proc Natl Acad Sci U S A 103:2428–2433. [PubMed: 16467152]

Mueller GP and Driscoll WJ (2007) In vitro synthesis of oleoylglycine by cytochrome c points to a novel pathway for the production of lipid signaling molecules. J Biol Chem 282:22364–22369. [PubMed: 17537719]

O'Byrne J, Hunt MC, Rai DK, Saeki M, and Alexson SE (2003) The human bile acid-CoA:amino acid N-acyltransferase functions in the conjugation of fatty acids to glycine. J Biol Chem 278:34237–34244. [PubMed: 12810727]

Prieto AL, O'Dell S, Varnum B, and Lai C (2007) Localization and signaling of the receptor protein tyrosine kinase Tyro3 in cortical and hippocampal neurons. Neuroscience 150:319–334. [PubMed: 17980494]

Ramsey IS, Delling M, and Clapham DE (2006) An introduction to TRP channels. Annu Rev Physiol 68:619–647. [PubMed: 16460286]

Rezgaoui M, Susens U, Ignatov A, Gelderblom M, Glassmeier G, Franke I, Urny J, Imai Y, Takahashi R, and Schaller HC (2006) The neuropeptide head activator is a high-affinity ligand for the orphan G-protein-coupled receptor GPR37. J Cell Sci 119:542–549. [PubMed: 16443751]

Rimmerman N, Hughes HV, Bradshaw HB, Pazos MX, Mackie K, Prieto AL, and Walker JM (2008) Compartmentalization of endocannabinoids into lipid rafts in a dorsal root ganglion cell line. Br J Pharmacol 153:380–389. [PubMed: 17965731]

Ritenour-Rodgers KJ, Driscoll WJ, Merkler KA, Merkler DJ, and Mueller GP (2000) Induction of peptidylglycine -amidating monooxygenase in N(18)TG(2) cells: a model for studying oleamide biosynthesis. Biochem Biophys Res Commun 267: 521–526. [PubMed: 10631094]

Ross RA (2003) Anandamide and vanilloid TRPV1 receptors. Br J Pharmacol 140: 790–801. [PubMed: 14517174]

Ross RA, Coutts AA, McFarlane SM, Anavi-Goffer S, Irving AJ, Pertwee RG, MacEwan DJ, and Scott RH (2001) Actions of cannabinoid receptor ligands on rat cultured sensory neurones: implications for antinociception. Neuropharmacology 40:221–232. [PubMed: 11114401]

Ryberg E, Larsson N, Sjogren S, Hjorth S, Hermansson NO, Leonova J, Elebring T, Nilsson K, Drmota T, and Greasley PJ (2007) The orphan receptor GPR55 is a novel cannabinoid receptor. Br J Pharmacol 152:1092–1101. [PubMed: 17876302]

Saghatelian A, McKinney MK, Bandell M, Patapoutian A, and Cravatt BF (2006) A FAAH-regulated class of N-acyl taurines that activates TRP ion channels. Biochemistry 45:9007–9015. [PubMed: 16866345]

Schachter D and Taggart JV (1954) Glycine N-acylase: purification and properties. J Biol Chem 208:263–275. [PubMed: 13174534]

Sheskin T, Hanus L, Slager J, Vogel Z, and Mechoulam R (1997) Structural requirements for binding of anandamide-type compounds to the brain cannabinoid receptor. J Med Chem 40:659–667. [PubMed: 9057852]

Ventura-Martínez R, Deciga-Campos M, Díaz-Reval MI, González-Trujano ME, and López-Muñoz FJ (2004) Peripheral involvement of the nitric oxide-cGMP pathway in the indomethacin-induced antinociception in rat. Eur J Pharmacol 503:43–48. [PubMed: 15496294]

Willis WD Jr (2007) The somatosensory system, with emphasis on structures important for pain. Brain Res Rev 55:297–313. [PubMed: 17604109]

Wink DA and Mitchell JB (1998) Chemical biology of nitric oxide: insights into regulatory, cytotoxic, and cytoprotective mechanisms of nitric oxide. Free Radic Biol Med 25:434–456. [PubMed: 9741580]

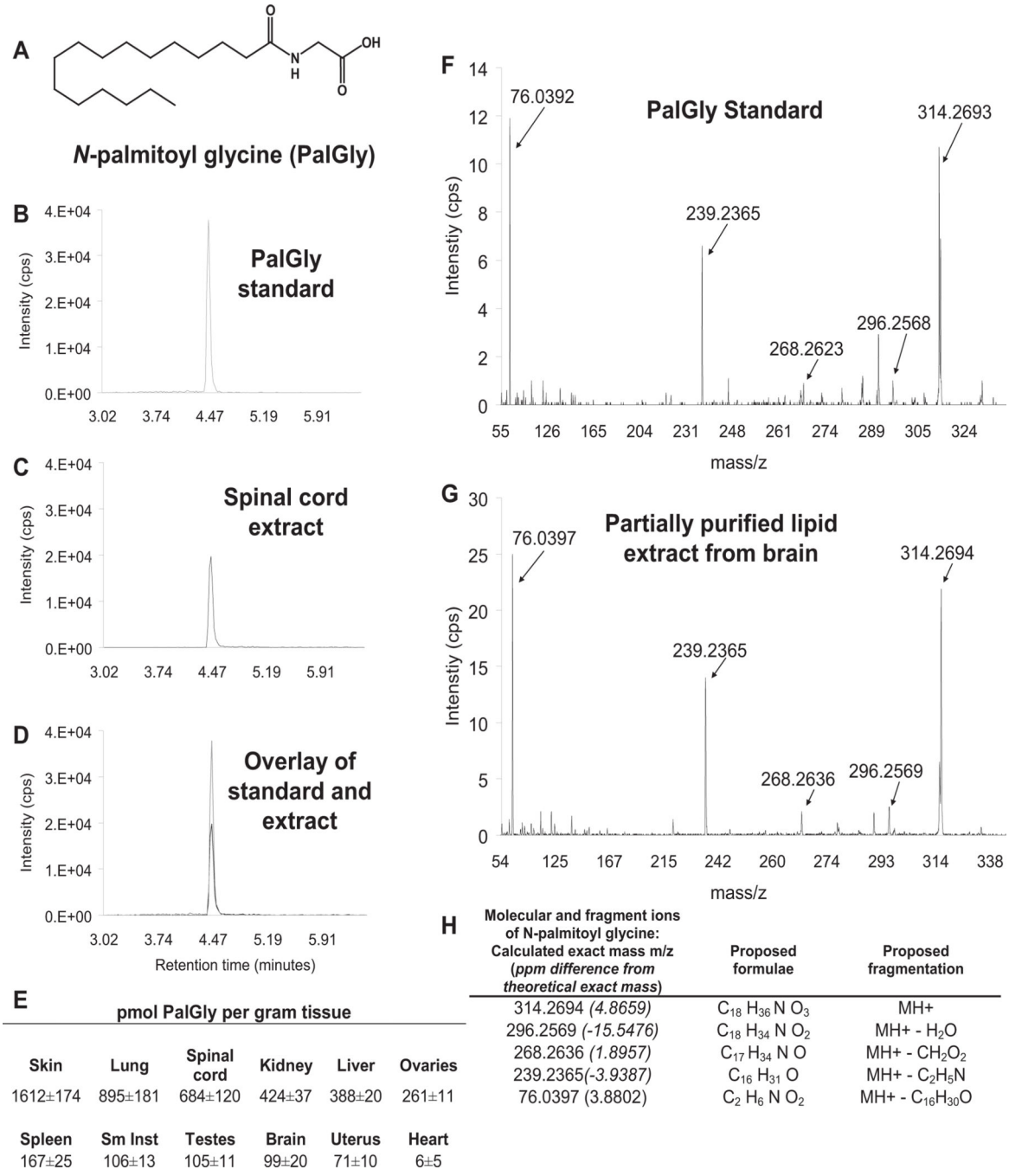

E

pmol PalGly per gram tissue

Skin	Lung	Spinal cord	Kidney	Liver	Ovaries
1612±174	895±181	684±120	424±37	388±20	261±11

Spleen	Sm Inst	Testes	Brain	Uterus	Heart
167±25	106±13	105±11	99±20	71±10	6±5

Fig. 1.

Chromatographic and mass spectrometric analysis revealed endogenous occurrence of *N*-palmitoyl glycine. A, PalGly: a 16-carbon saturated fatty acid conjugated to a glycine molecule through an amide bond. B, 500-fmol standard of PalGly using the LC/MS/MS MRM method and chromatographic gradient outlined under Materials and Methods. C, 10-*μ*l injection of lipid extract from spinal cord using the same PalGly LC/MS/MS MRM method described in C. D, overlay of chromatograms from B and C. E, constitutive production of PalGly was measured in partially purified lipid extracts using LC/MS/MS

using MRM methods. Values are reported as pmol/g dry tissue (mean ± S.E.M.), estimated from the ratio of lyophilized to wet weight of each type of tissue. Sm Inst, small intestine. F, product ion scan mass spectrum of the positively charged molecular ion of the PalGly synthetic standard in which the arrows are directed to the peaks of the proposed molecular and fragment ions and labeled with the calculated exact mass. G, product ion scan mass spectrum of the brain lipid extract tuned to the positively charged PalGly molecular ion in which the arrows are directed to the peaks of the proposed molecular and fragment ions and labeled with the calculated exact mass. H, mass measurements of the molecular and fragment ions together with the proposed formulae of these ions for PalGly found in lipid extract from murine brain. The parts per million (ppm) differences from the theoretical exact masses of each molecular ion and fragment ion are represented in parentheses.

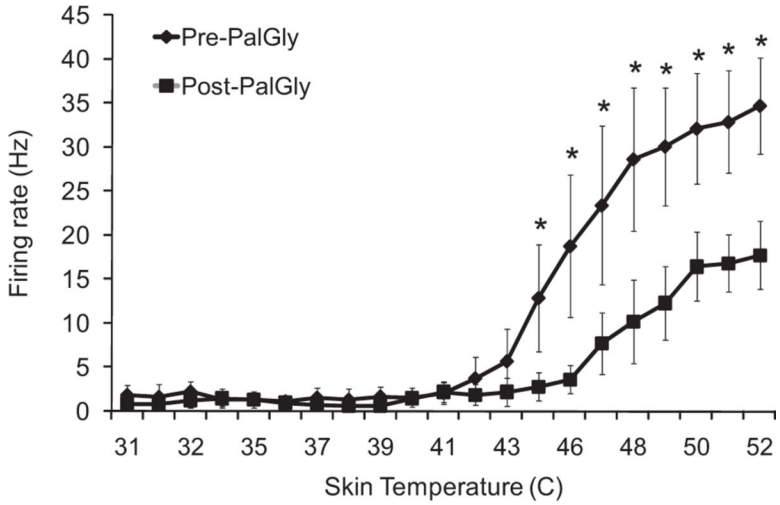

Fig. 2.

Peripheral administration of PalGly suppressed heat-evoked firing in spinal nociceptive neurons. Firing rates of WDR neurons in response to exposure of their receptive fields to a heat ramp. Heat-evoked firing rates were measured before and 30 min after intradermal injection of PalGly (0.43 μg). Mean firing rates were calculated before (pre) and after (post) PalGly administration. *, $p < 0.05$ difference from pre-PalGly firing rates. Error bars indicate standard error of the mean.

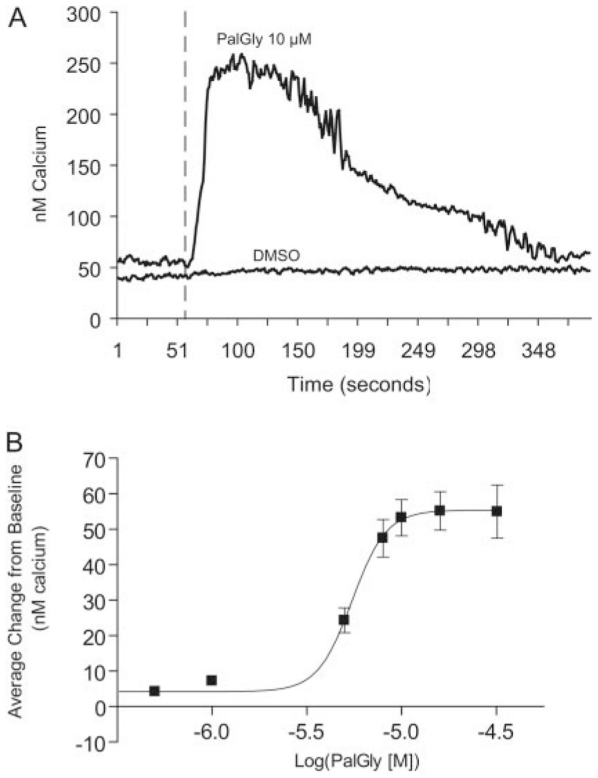

Fig. 3.

PalGly induced a dose-dependent calcium influx in F-11 cells. A, single cell calcium traces (assessed by Fura-2 fluorescence) of F-11 cells treated with either 10 μM PalGly or DMSO. Dashed line indicates the time of drug administration. B, a dose-response curve of F-11 cells to PalGly. The following formula was used to calculate the average change in nanomolar calcium for each cell: [(the average response 60 s after PalGly application) – (the average response 60 s before PalGly application)]. All cells, regardless of their response rate, were averaged. Each data point represents an average of single cells (n = 31–75) from at least three independent plates. The EC_{50} value for PalGly = 5.5 μM. Error bars indicate S.E.M.

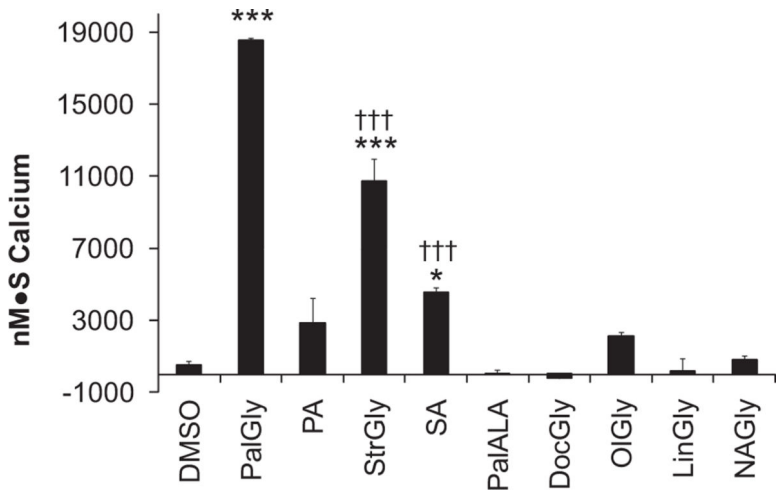

Fig. 4.

PalGly induced calcium influx in F-11 cells with strict structural requirements. Comparison of PalGly-induced calcium influx with calcium influx by structurally related molecules. Calcium influx was calculated from the integral of the time × calcium-concentration curve as described in the text. Free glycine was tested at 16 μM. All other compounds were tested at 10 μM. One-way ANOVA with Bonferroni's post hoc test. *, $p < 0.05$ compared with vehicle; ***, $p < 0.001$ compared with vehicle; †††, $p < 0.001$ compared with PalGly.

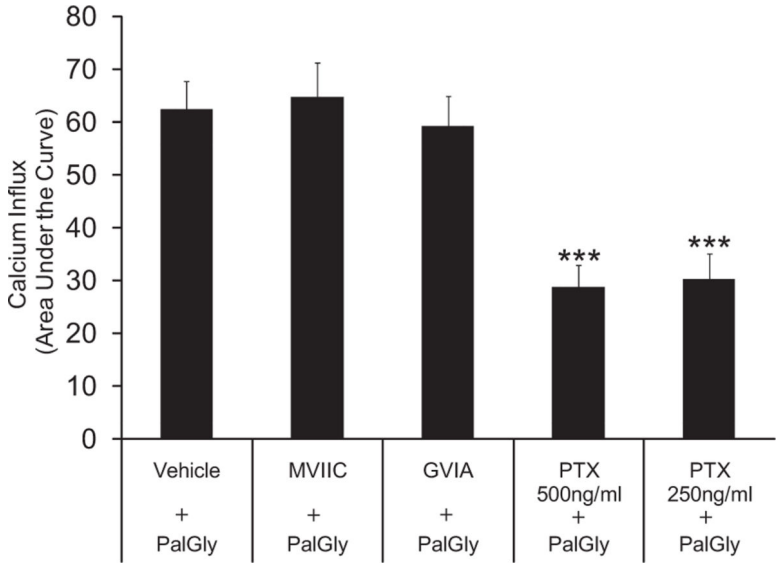

Fig. 5.

PTX attenuated PalGly-induced calcium influx. The effect of PalGly (15 μM) was significantly attenuated by pertussis toxin (250 or 500 ng/ml) but not by ω-conotoxin MVIIC (2 μM) or ω-conotoxin GVIA (2 M). ω-Conotoxin MVIIC and ω-conotoxin GVIA were tested in the presence of fatty acid-free bovine serum albumin. Calcium influx was calculated by integrating the area under 340/380 fluorescence ratio × time curves. $n = 8$ wells per condition, ***, $p < 0.001$ difference from vehicle + PalGly. One-way ANOVA with LSD post hoc tests. Error bars indicate standard error of the mean.

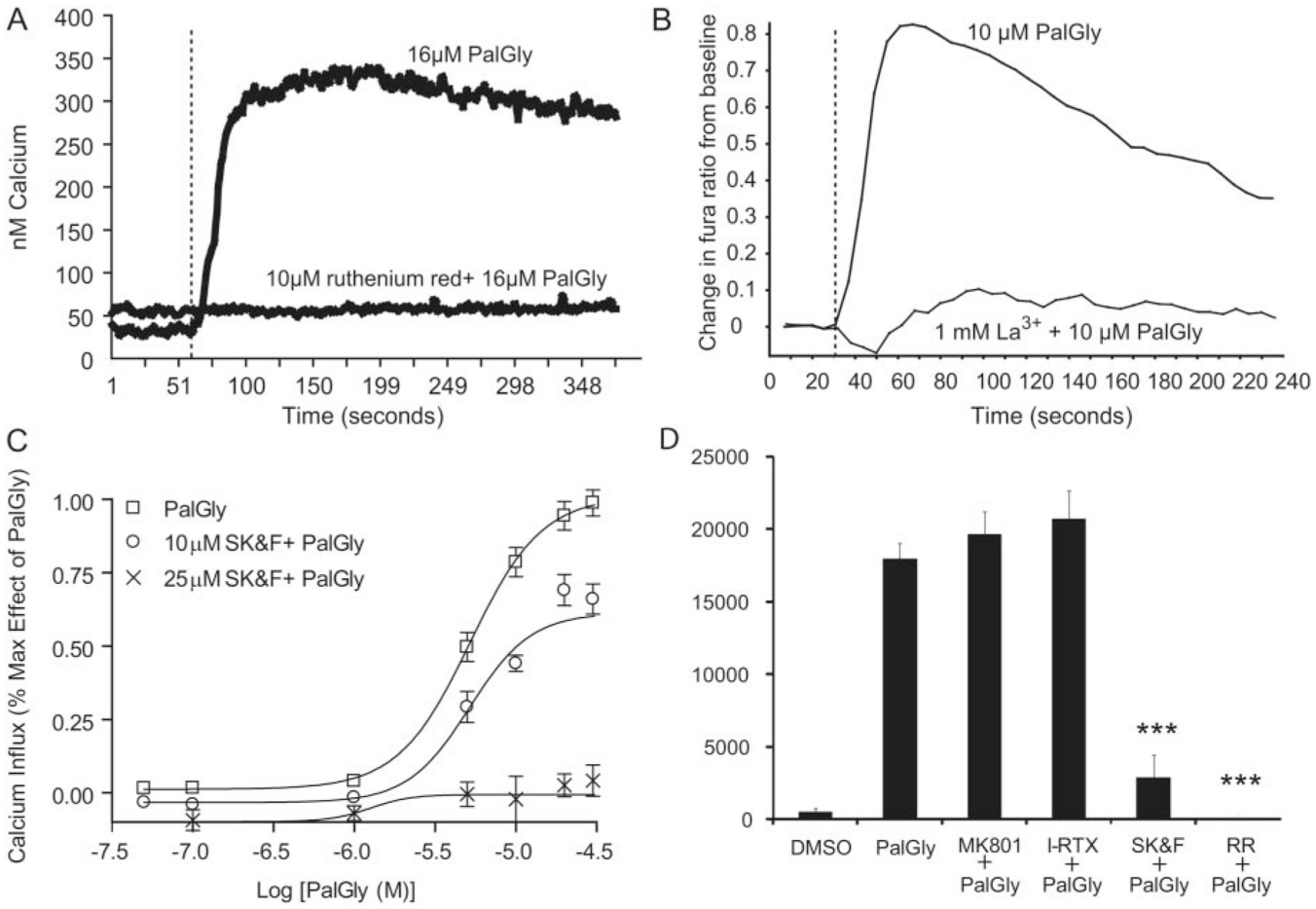

Fig. 6.

PalGly-induced calcium influx was inhibited by pretreatment with ruthenium red (10 M), SK&F96365 (25 μM), and La^{3+} (1 mM). A, single cell calcium traces for F-11 cells treated with 16 μM PalGly after administration of vehicle or 10 μM ruthenium red. B, a representative F-11 well population calcium influx of cells pretreated with La^{3+} or vehicle. C, concentration-response curves for PalGly and PalGly + SK&F96365 (10 or 25 μM) show profound inhibition of PalGly-induced calcium influx in F-11 cells after treatment with 25 μM SK&F96365. n = 3–20 wells per condition. D, PalGly (16 μM) induced marked calcium influx in the presence of MK801 (25 μM) and I-RTX (35 nM), whereas it lacked efficacy in the presence of SK&F96365 (10 and 24 μM) or ruthenium red (10 μM). Calcium mobilization was calculated from the integral of the calcium concentration × time curve as described in the text. ***, $p < 0.001$ difference from vehicle + PalGly. One-way ANOVA with LSD post hoc tests. Error bars indicate S.E.M.

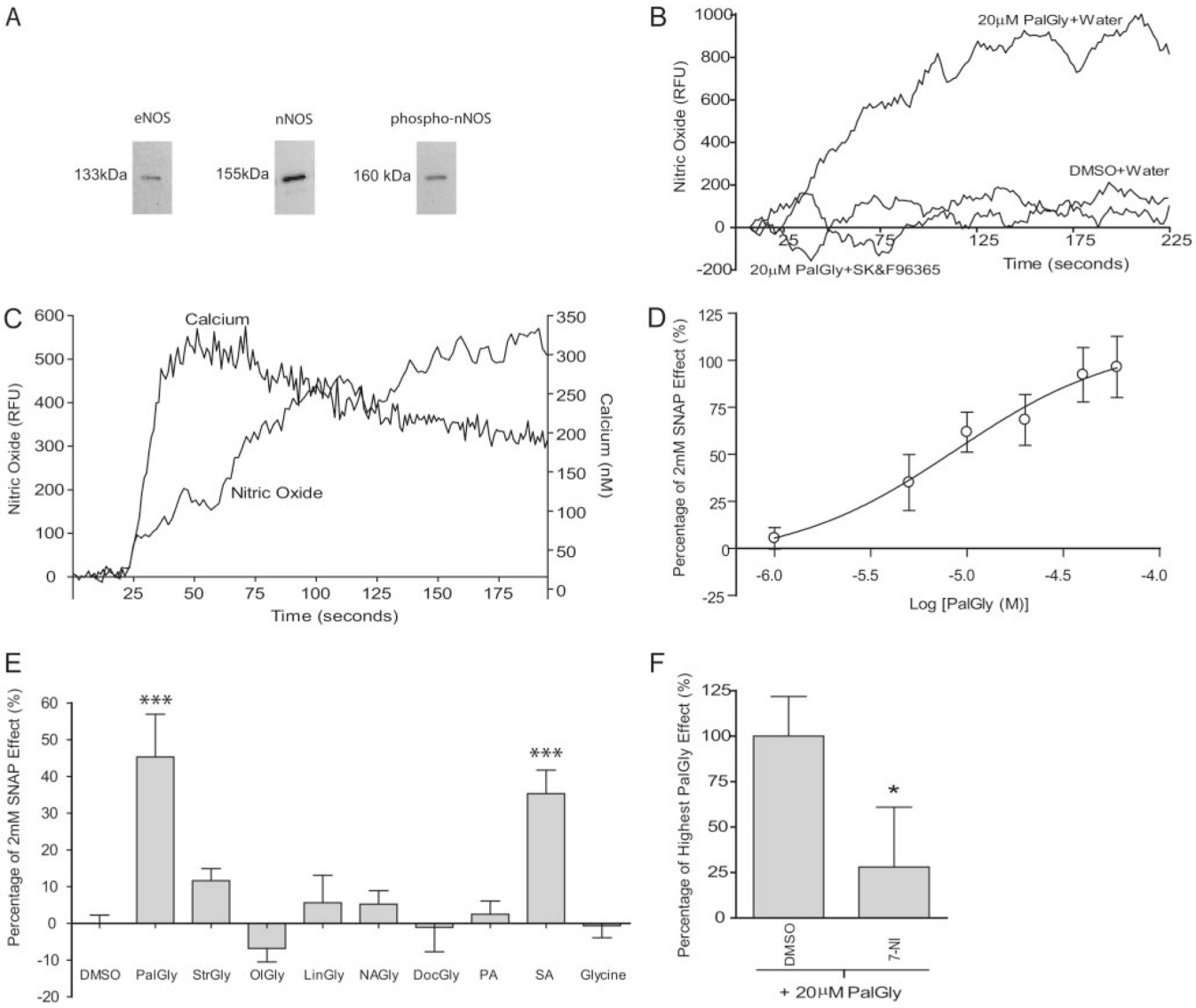

Fig. 7.

PalGly treatment induced NO production in F-11 cells in a calcium-dependent manner. A, F-11 cells express calcium-dependent NOS isoforms. Western blots showed that eNOS, nNOS, and Ser847-phospho-nNOS were present in F-11 cells. iNOS was not detected using Western blotting. B, NO release by F-11 cells upon PalGly treatment is calcium channel-dependent. Traces from individual wells containing DAF-2-loaded F-11 cells displayed an increase in NO upon treatment with PalGly but not DMSO. Treatment of F-11 cells with the nonspecific calcium channel blocker SK&F96365 (20 M) suppressed PalGly-evoked NO release compared with vehicle (water)-treated cells. Data points are presented as the increase in fluorescence relative to baseline using a 9-point moving point average. C, NO production closely parallels calcium influx in F-11 cells. A calcium trace from a single cell is overlaid with a NO trace from a single well. D, PalGly causes dose-dependent release of NO in F-11 cells. Data are presented as a percentage of the effect of 2 mM SNAP in 5 μM DAF-2. PalGly at and above 10 μM caused significant elevations in NO release compared with

DMSO (**, $p < 0.01$, $n = 6$, one-way ANOVA, Dunnett's t test, post hoc). The EC_{50} value for the effect of PalGly was 8.7 μM. E, NO release by PalGly in F-11 cells had rigid structural requirements. PalGly and stearic acid (SA), but not other structurally related compounds, significantly increased NO production compared with DMSO vehicle (***, $p < 0.001$, $n \geq 9$, one-way ANOVA, Dunnett's t test, post hoc). All compounds were tested at 10 μM. Data are presented as a percentage of the effect of 2 mM SNAP in 5 μM DAF-2. F, NOS catalyzes PalGly-induced NO production. PalGly-induced NO production in F-11 cells was inhibited by pretreatment of cells with 200 μM 7-NI, a NOS inhibitor (*, $p < 0.05$, $n = 32$, one-way ANOVA, LSD post hoc test). Data are presented as a percentage of the maximum mean effect of PalGly in each experiment, which occurred in each case under DMSO treatment conditions. Error bars represent S.E.M.

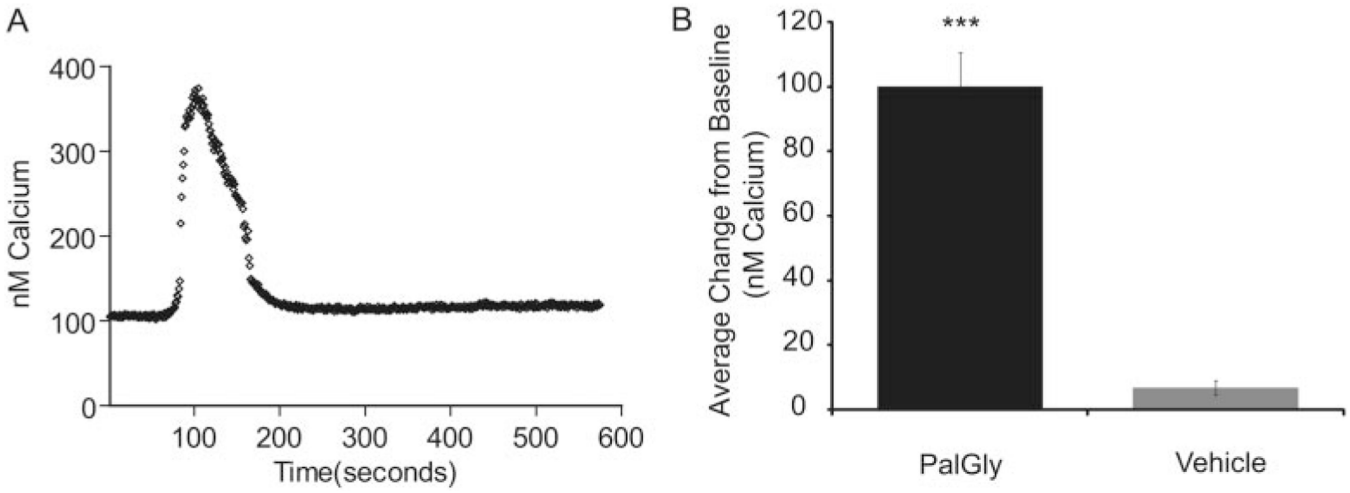

Fig. 8.

PalGly-induced calcium influx in a large subset of native adult DRG cells. A, a single cell trace of a primary adult DRG cell treated with PalGly (16 μM) after 60 s of baseline recording. B, average increase in calcium influx after PalGly application (for cells that responded with an average >50 nM calcium increase over baseline), was significantly different from the average increase after vehicle treatment [total cells; C; $t(54) = 12.4$; two-tailed; ***, $p < 0.001$].